Electronic Supplementary Material (ESI) for Journal of Materials Chemistry C.

Green Syntheses of Stable and Efficient Organic Dyes for Organic Hybrid Light-Emitting Diodes

Yunping Huang,[a] Theodore A. Cohen[b], Parker J. W, Sommerville[c] and Christine K. Luscombe*[abc]

[a.] Department of Materials Science & Engineering, University of Washington, Seattle, WA 98195, USA.

[b.] Molecular Engineering & Sciences Institute, University of Washington, Seattle, WA 98195, USA.

[c.] Department of Chemistry, University of Washington, Seattle, WA 98195, USA.

Table of Contents

1. Synthetic procedures and NMR spectra and mass spectra

Theobromine, 1-bromooctane, R305 DCJTB, 4,7-dibromo-benzo[c][1,2,5]thiadiazole were purchase from TCI. Bis(dibenzylideneacetone)palladium(0) anhydrous xylene and pivalic acid were purchased from Sigma Aldrich. K_2CO_3 and Cs_2CO_3 were ground into a powder and dried at 120 °C overnight before reactions. Reactions were run under N_2 atmosphere using standard Schlenk techniques and detailed synthesis procedures are described below. Theo8[1] and 4,7-dibromobenzo[c][1,2,5]thiadiazole[2] were prepared according to literature procedures. NMR was taken with Bruker 500 MHz spectrometer.

8,8'-(benzo[*c*][1,2,5]thiadiazole-4,7-diyl)bis(3,7-dimethyl-1-octyl-3,4,5,7-tetrahydro-1H-purine-2,6-dione) (Theo-Green). Theo8 (1,932 mg, 7 mmol) and 4,7-dibromobenzo[*c*][1,2,5]thiadiazole (873 mg, 3 mmol), pivalic acid (80 mg, 0.8 mmol) and dried Cs_2CO_3 (3 g, 9 mmol) were added into a 50 mL round bottom flask. 25 mL *o*-xylene was then adding into the flask, followed by degassing with N_2 flow for 10 min. Tris(2-methoxyphenyl)phosphine (122 mg, 0.194 mmol) and bis(dibenzylideneacetone)palladium(0) (80 mg, 0.088 mmol) were added to the solution under N_2 flow, and the solution turned purple. The flask was then sealed with a rubber stopper and heated to 100 °C. After reacting for 1 day, the system was cooled and filtered. The organic phase was then concentrated under reduced pressure. The crude product was further purified with column chromatography using dichloromethane/methanol in a ratio of 40/5 as an eluent. 1.31 g yellow solid was obtained in 61% yield. ^{1}H NMR (500 MHz, Chloroform-*d*) δ 8.10 (s, 2H), 4.10 – 4.02 (m, 4H), 4.00 (s, 6H), 3.64 (s, 6H), 1.75 – 1.63 (m, 4H), 1.47 – 1.21 (m, 20H), 0.91 – 0.84 (m, 6H). ^{13}C NMR (126 MHz, $CDCl_3$) δ 155.93, 153.11, 151.88, 148.87, 148.10, 132.60, 124.81, 110.04, 42.15, 34.79, 32.30, 30.26, 29.72, 28.62, 27.52, 23.12, 14.56.

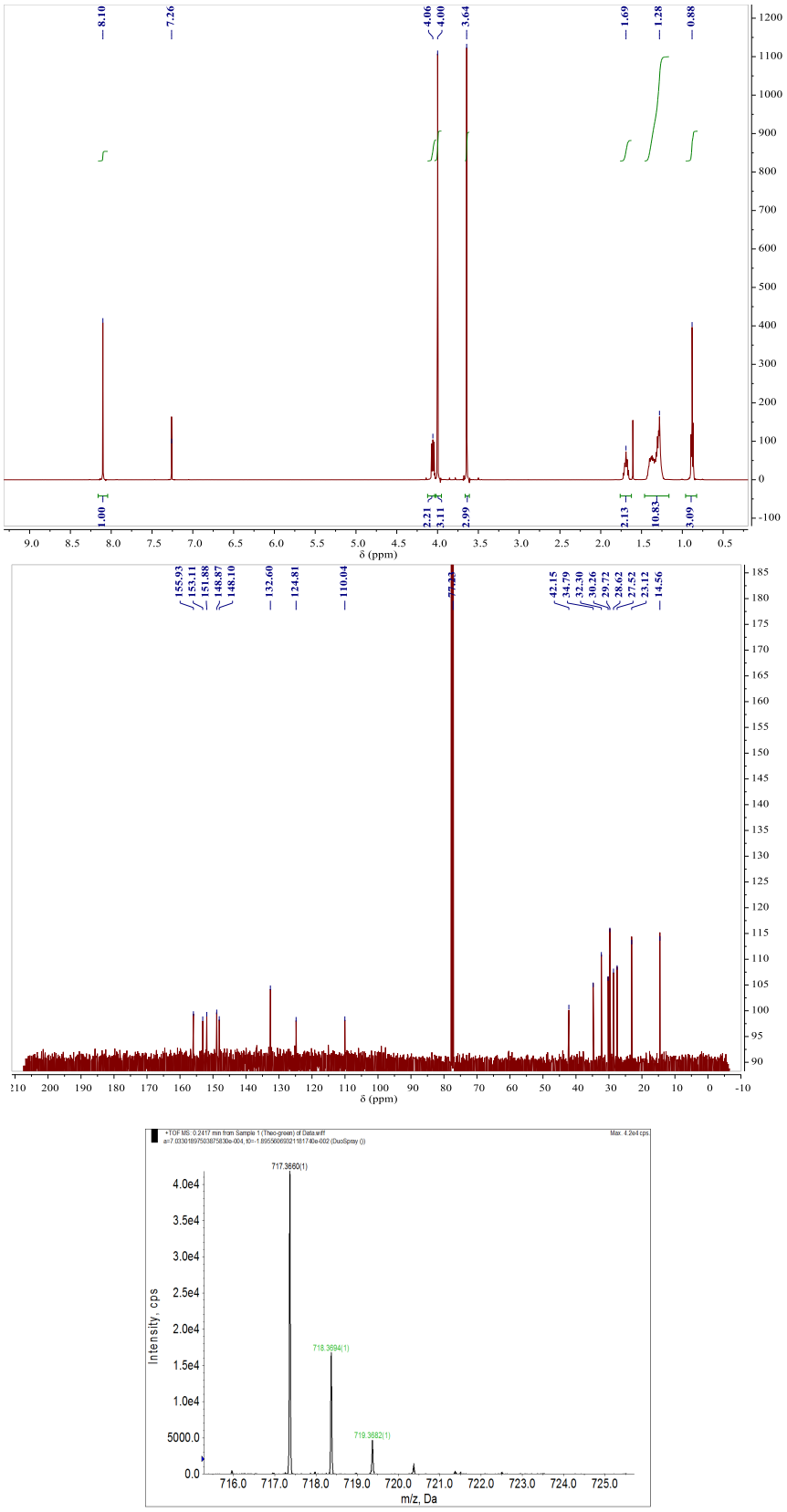

Fig. S1.1. (top) ^{1}H NMR, (middle) ^{13}C NMR and (bottom) mass spectra of Theo-Green.

8,8'-(naphtho[2,3-c][1,2,5]thiadiazole-4,9-diyl)bis(3,7-dimethyl-1-octyl-3,4,5,7-tetrahydro-1H-purine-2,6-dione) (Theo-Red). Theo8 (1,932 mg, 7 mmol) and 4,7-dibromobenzo[*c*][1,2,5]thiadiazole (1,032 mg, 3 mmol), pivalic acid (80 mg, 0.8 mmol) and dried Cs_2CO_3 (3 g, 9 mmol) were added into a 50 mL round bottom flask. 25 mL *o*-xylene was then adding into the flask, followed by degassing with N_2 flow for 10 min. Tris(2-methoxyphenyl)phosphine (122 mg, 0.194 mmol) and bis(dibenzylideneacetone)palladium(0) (80 mg, 0.088 mmol) were added to the solution under N_2 flow, and the solution turned purple. The flask was then sealed with a rubber stopper and heated to 100 °C. After reacting for 1 day, the system was cooled and filtered. The organic phase was then concentrated under reduced pressure. The crude product was further purified with column chromatography using dichloromethane/methanol in a ratio of 40/5 as an eluent. 1.20 g red solid was obtained in 52% yield. ^{1}H NMR (500 MHz, Chloroform-*d*) δ 7.97 (ddd, 2H), 7.72 – 7.48 (m, 2H), 4.19 – 3.98 (m, 4H), 3.82 (s, 6H), 3.67 (s, 6H), 1.91 – 1.63 (m, 4H), 1.50 – 1.21 (m, 20H), 0.94 – 0.77 (m, 6H). ^{13}C NMR (126 MHz, $CDCl_3$) δ 155.88, 151.91, 151.46, 148.96, 146.98, 134.70, 129.75, 126.76, 119.65, 109.58, 42.19, 33.95, 32.31, 30.37, 29.73, 28.64, 27.55, 23.12, 14.58.

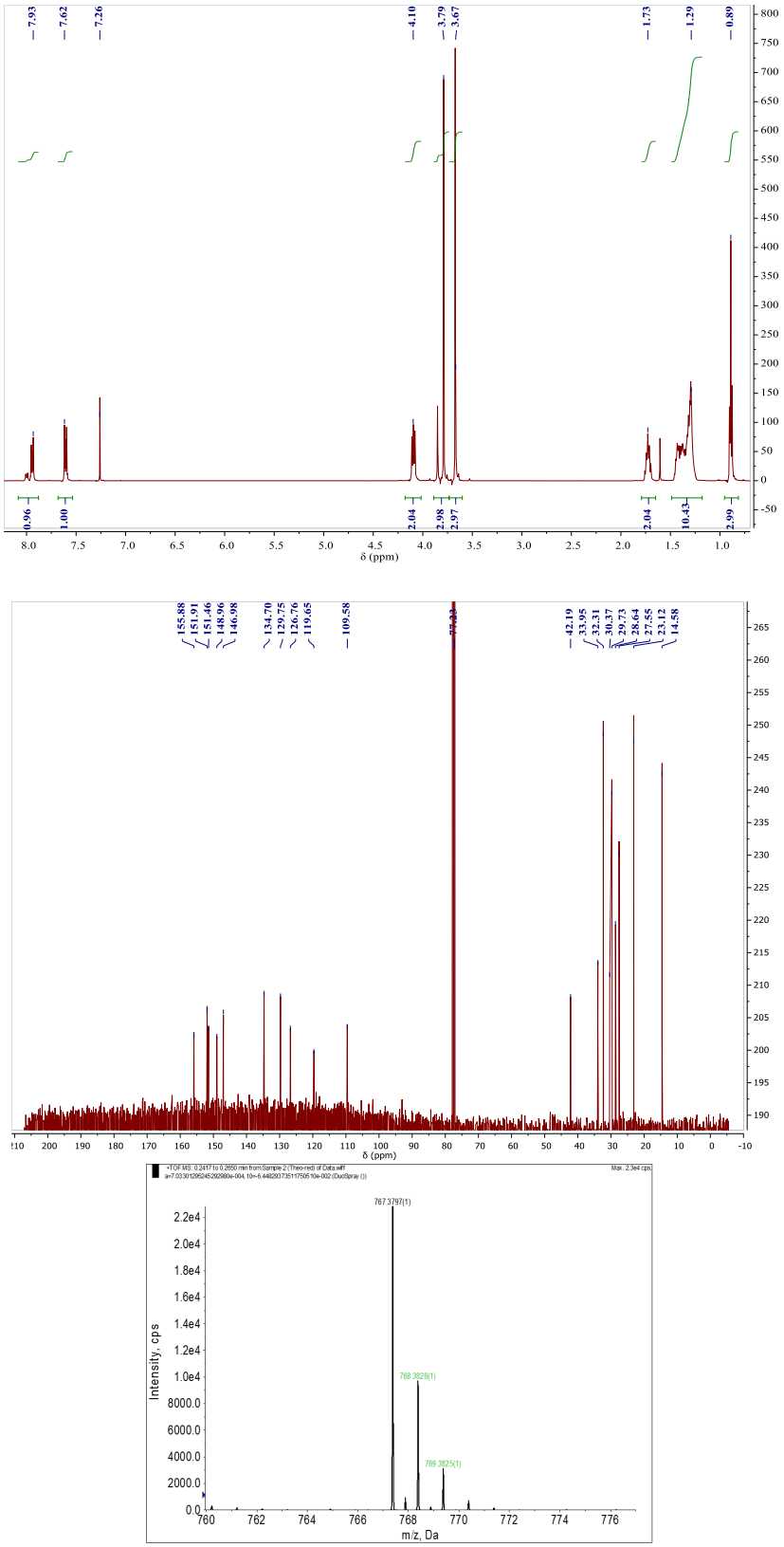

Fig. S1.2. (top) ^{1}H NMR, (middle) ^{13}C NMR and (bottom) mass spectra of Theo-Red.

2. Density functional theory calculation results

Chemical structures of all three molecules were imported from Chemdraw into Gaussview 5.0. Density functional theory calculations were performed using the Gaussian 16 (Revision b.01) software package. Structure optimizations were performed under the B3LYP functional and 6-31g (d) basis set. Once the optimization was complete, the saved checkpoint files were converted to form check files before being converted to cube files using the cubegen utility. The cube files were opened in Gaussview 5.0 and images of the molecular orbitals of each molecule were taken. This work was facilitated through the use of advanced computational, storage, and networking infrastructure provided by the Hyak supercomputer system and funded by the STF at the University of Washington.

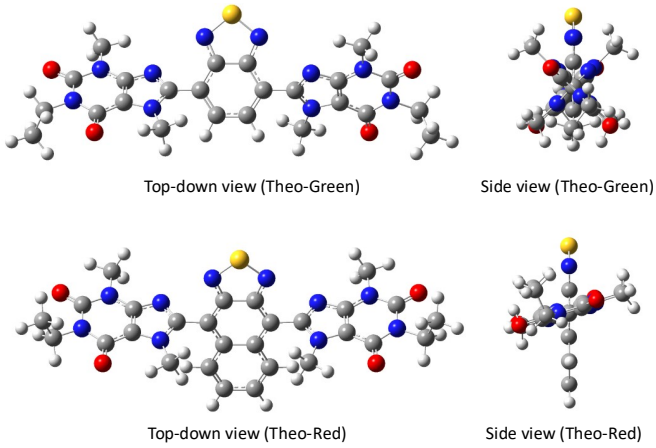

Fig. S2.1. Optimized geometry of Theo-Green and Theo-Red.

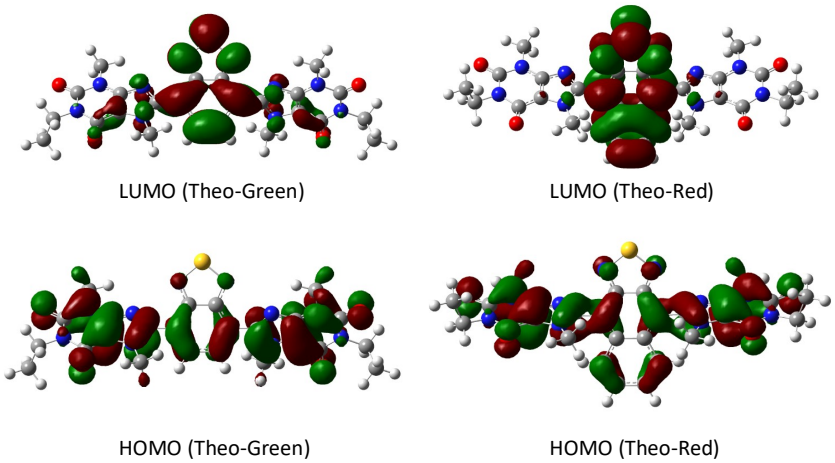

Fig. S2.2. Frontial molecule orbitals of Theo-Green and Theo-Red.

3. Full UPS spectra of the six organic dyes

Sample preparation: ITO substrates were sonicated in acetone and iso-propanol respectively for 15 mins and then dried by air. They were then cleaned using an ozone plasma for 15 min. Organic dye chloroform solutions (30 mg/ml) were then spincoated onto the clean ITO at 2000 rpm for 30 s under ambient conditions. The obtained samples were dried overnight under high vacuum. UPS spectra were obtained with Kratos AXIS Ultra DLD with He (I) source and pass energy of 5 eV.

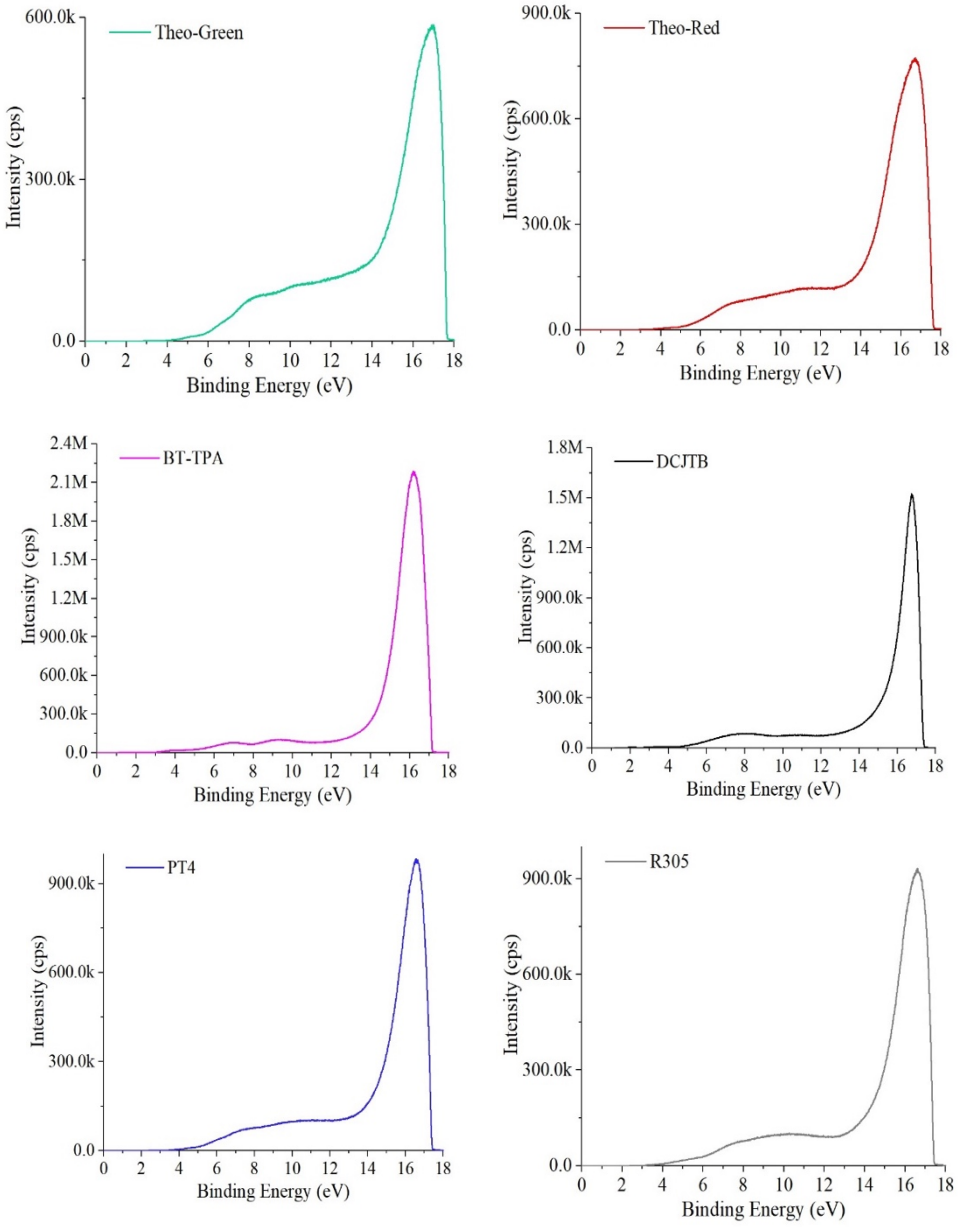

Fig. S3. UPS spectra of six dyes.

4. Thin film absorptions of six organic dyes

Sample preparation: Organic dye chloroform solutions (20 mg/ml) were spincoated onto glass substrate at 1000 rpm for 60 s under ambient conditions. The obtained samples were dried overnight under high vacuum of 10^{-7} mbar. Absorption spectra were taken with Perkin Elmer Lambda 950 – UV Vis/NIR spectrophotometer. PLQY data were obtained using an integrating sphere (Hamamatsu, C9920-12).

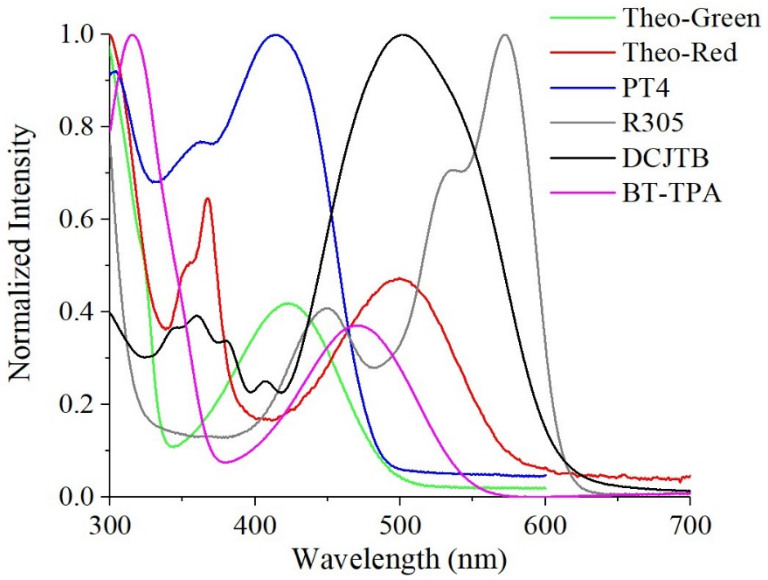

Fig. S4. Thin films absorption of organic dyes.

Table S1. Energetic parameters of the six organic molecules.

	HOS [eV][a)]	Band 1 [eV][a)]	Band 2 [eV][a)]	Cutoff [eV][a)]	HOMO-top [eV][b)]	HOMO-1 [eV][b)]	HOMO-2 [eV][b)]	Abs λ_{cutoff} [nm][c)]	Eg [eV][d)]	LUMO-bottom [eV][e)]
Theo-Green	2.20	4.44	5.76	17.64	-5.76	-8.00	-9.32	505	2.46	-3.30
Theo-Red	2.05	3.51	4.72	17.61	-5.64	-7.10	-8.31	590	2.10	-3.54
BT-TPA	0.92	1.75	4.07	17.18	-4.94	-5.77	-8.09	561	2.21	-2.73
DCJTB	1.03	2.00	3.76	17.38	-4.85	-5.82	-7.58	627	1.98	-2.87
PT4	1.90	3.61	4.81	17.41	-5.69	-7.40	-8.60	485	2.56	-3.13
R305	1.90	3.66	4.78	17.44	-5.66	-7.42	-8.54	620	2.00	-3.66

[a)] Obtained from UPS results in Figure 4; [b)] Calculated from the UPS results based on $E_{Top,HOMO} = -21.2\ eV + (E_{Cutoff} - E_{HOS})$; [c)] Obtained from UV-vis spectra in Figure S3.1; [d)] Calculated based on $E_g = \frac{1240}{\lambda_{cutoff}}$; e) Calculated based on $E_{Bottom,LUMO} = E_{Top,HOMO} + E_g$.

5. Stability comparison between neat organic dye thin films and organic dye SBS complex

Neat organic thin film preparation: Organic dye chloroform solutions (20 mg/ml) were spincoated on glass substrate at 1000 rpm for 60 s under ambient conditions. The obtained samples were then dried overnight under high vacuum of 10^{-7} mbar.

SBS complex preparation: At ambient air, organic dye and SBS were dissolved in toluene (dye : SBS : toluene = 1 mg : 100 mg : 1 ml). After the SBS fully dissolved, 300 µl of the clear solution was dropcast onto a 1.8 × 1.8 cm^2 glass substrate and dried under air flow. The obtained samples were then dried overnight under high vacuum of 10^{-7} mbar. (SBS were purchased from Sigma Aldrich, styrene 30 wt. %, average Mw ~140,000 by GPC, contains <0.5 wt. % antioxidant).

Dye stabilities under irradiation were measured with a homebuilt LED irradiation setup described previously.[3] Briefly, a Chanzon 50 W, 450 nm LED source was mounted inside an enclosed light box with a heat sink and a cooling fan. The sample and an optical fiber fixed near the edge of the sample were mounted below the LED such that the LED and the sample could be separated by a mechanical shutter. PL spectra were measured through the optical fiber with an ASEQ Instruments LR1-T spectrometer. Spectra were collected every 3 s for the first ~10 minutes of irradiation and every 5 minutes for the remainder of the experiment. Spectra were then integrated from 500 nm to 700 nm to obtain the integrated PL intensity as a function of irradiation time. The fluence incident on the sample was measured with a Coherent energy meter through a 1 mm diameter pinhole.

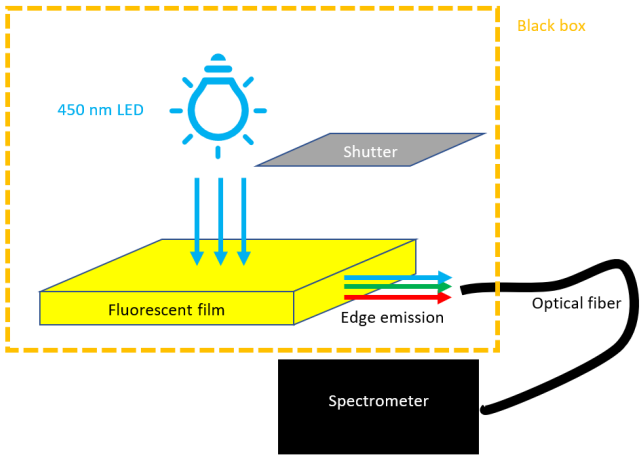

Fig. S5.1. Setup for the stability measurement.

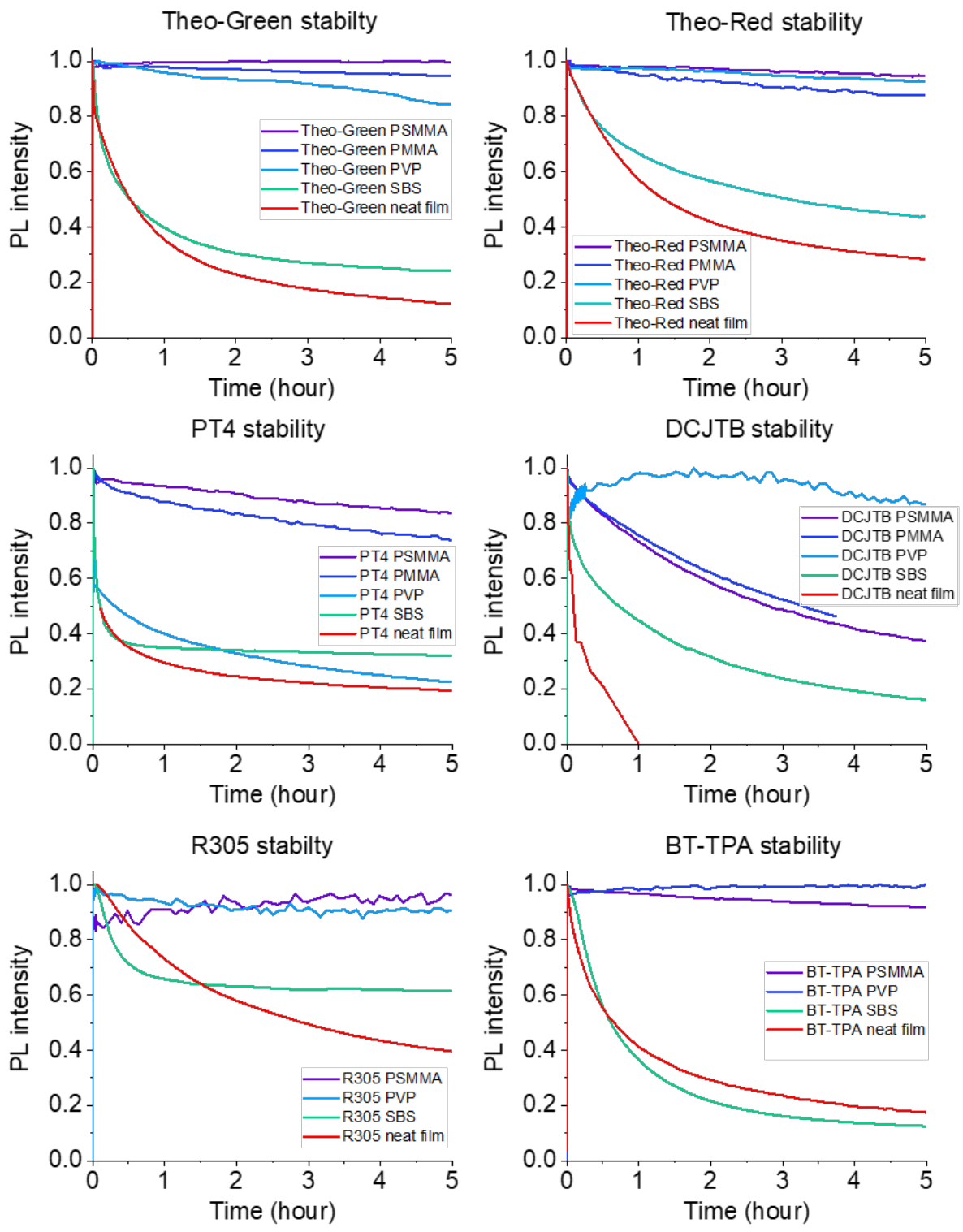

Fig. S5.2. Stability results of the organic dyes samples (as thin films and in different polymer matrices).

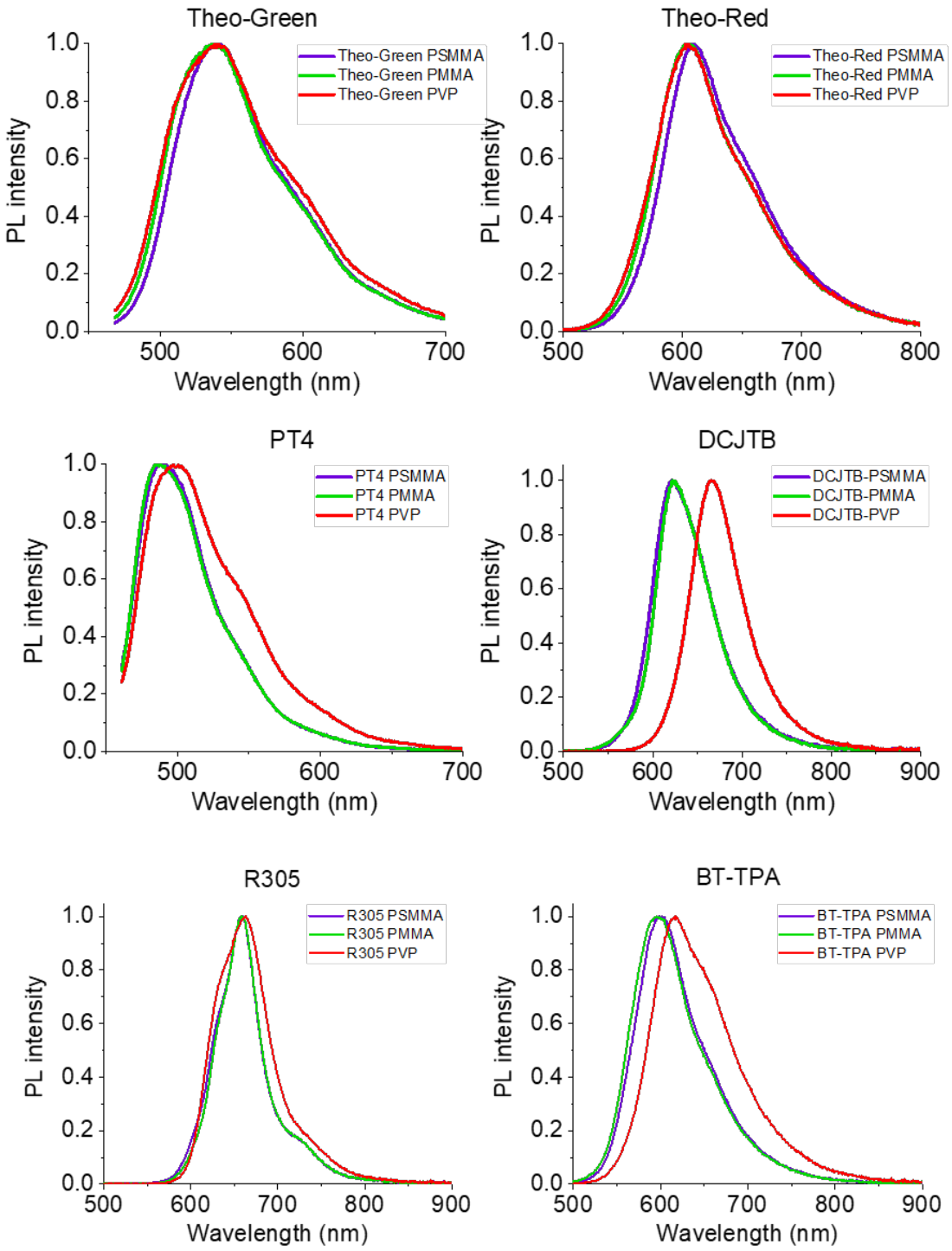

Fig. S5.3. PL spectra of organic dyes in polymer matrices of different polarity at 1:100 blending ratio.

In Fig. S5.2, we also included the stability studies of the six dyes in these polymers and we observed the two roles that the polymer matrix plays in the photostability of organic dyes. First, polymers that possess lower oxygen permeability deliver larger stability enhancement to the dye-polymer composite. SBS, which is the only elastomer among the polymers studied here, has much larger oxygen permeability compared to other polymers due to more free volume, and therefore delivers less stability enhancement when an organic dye is blended within. (Polymers 2019, 11, 1056.) Second, the polarity relation between dye and polymer plays an important role in the stability of the dye-polymer composite. Polar polymers provide larger stability improvements for dyes with strong charge transfer features (e.g., BT-TPA and DCJTB), while apolar polymers provide larger stability enhancements for dyes without strong charge transfer features (e.g., Theo-Green, Theo-Red, PT4 and R305).

6. Monitoring singlet oxygen generation

Procedure: An organic dye (0.005 mmol) and the singlet oxygen scavenger (diphenyl anthracene) (0.005 mmol) was weighed and added into a beaker, and 50 ml anisole was added to the beaker resulting in a clear solution. The dye concentration and scavenger concentration were both 10^{-4} M. The same procedure was repeated for the other organic dyes.

The resulting solutions in beakers were radiated in open air with a 450 nm LED of ~90 mW/cm^2, and solution samples were collected from the beaker at 0, 20, 40, 60, 80 and 100 min.

The UV-vis spectra of these collected samples were measured, with 10^{-4} M anisole solution of respective dyes as reference, so that we could directly monitor the changes in the diphenyl anthracene absorption. With the presence of singlet oxygen, diphenyl anthracene will be consumed (Scheme S1) and thus will lose its absorption features in the ultraviolet region.[4] As shown in Figure S6, there is no noticeable decay in the diphenyl anthracene absorptions in all six samples.

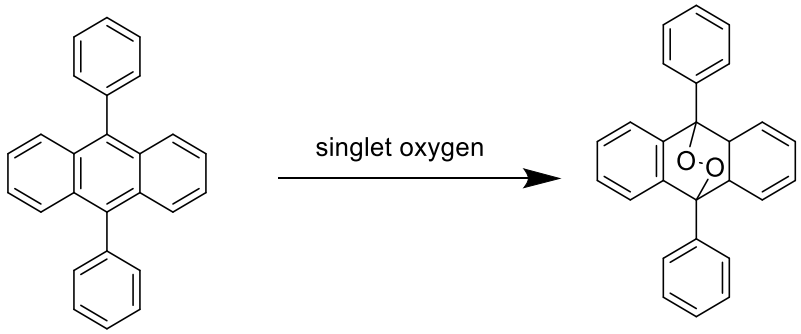

Scheme S1. The singlet oxygen scavenging mechanism of diphenyl anthracene.

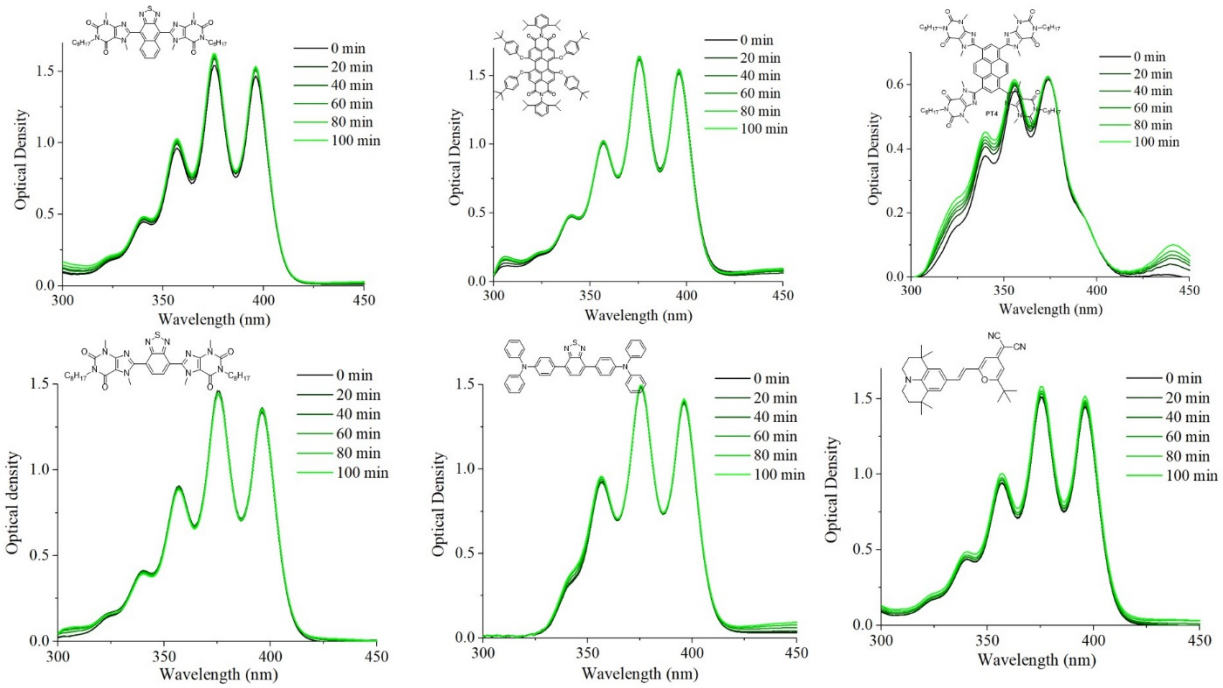

Fig. S6. The monitoring of singlet oxygen generation from the six organic dyes.

7. Particle size comparison of convertor-SBS composite

The bright field optical images were obtained via Nikon Eclipse LV150N. For all the organic dyes, only Theo-Green maintain a homogeneous morphology at 10 wt% blending ratio; Theo-Red starts to form fine aggregates and we obverse large crystal formation in BT-TPA-SBS composite. DCJTB and R305 forms aggregates at low concentration at 1 wt%. SGA isiphor is insoluble and the image shows a inhomogeneous morphology.

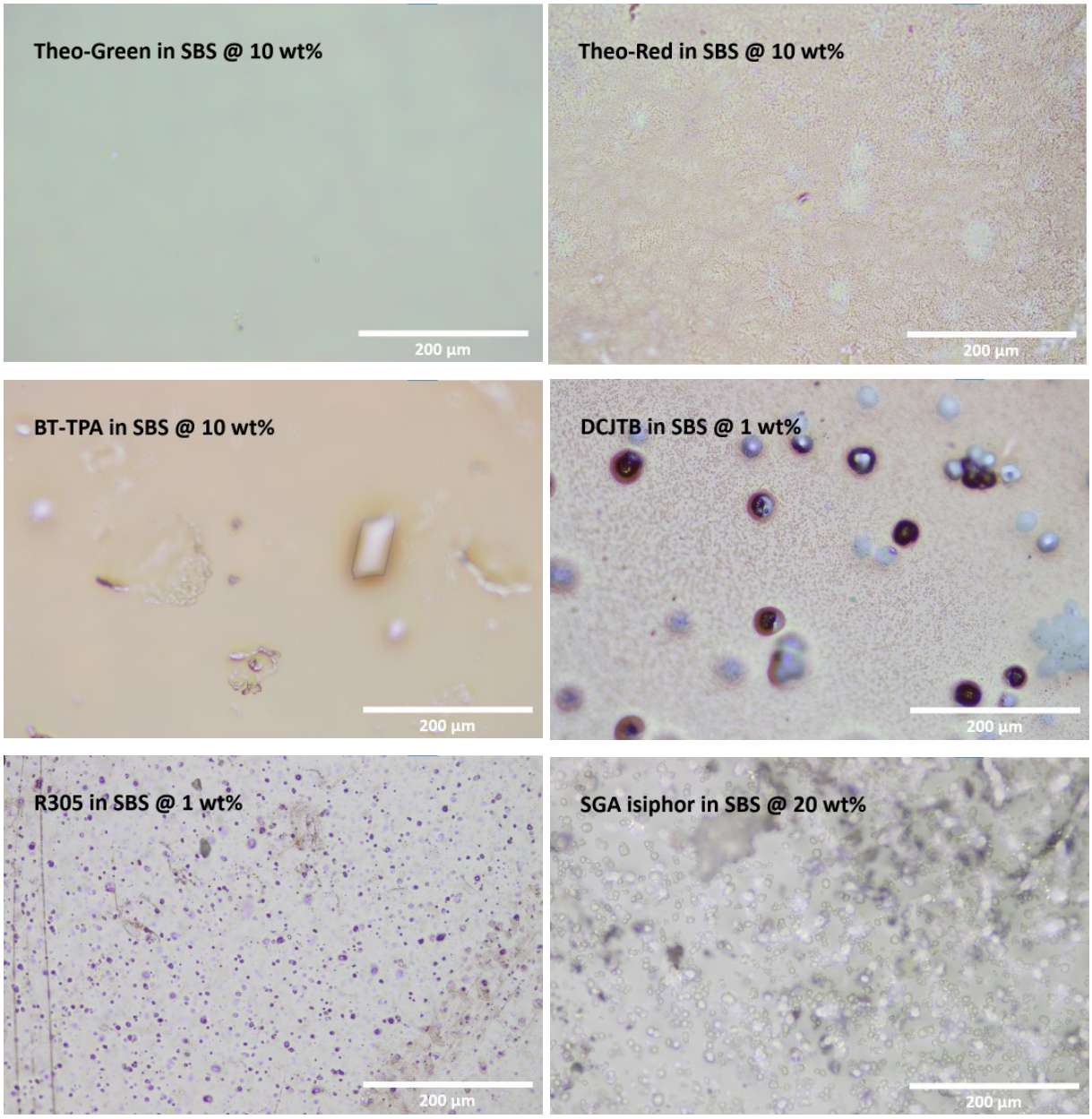

Fig. S7. Images of the lighting converting composites under optical microscope.

8. Emission of Theo-Green and Theo-Red in different blending concentration

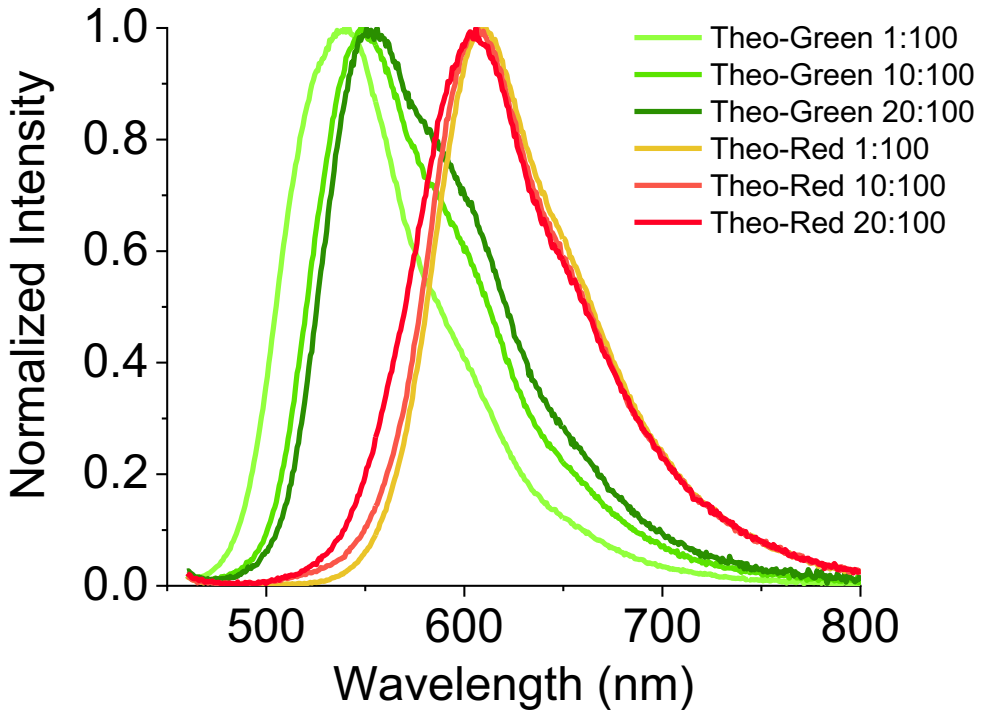

Fig. S8. The emission spectra of Theo-Green and Theo-Red SBS composites with different blending ratio.

Because of the differences in solubility, the PL of Theo-Green and Theo-Red show different trends as the dye-SBS ratio increase. Theo-Green forms transparent films with SBS even at a high blending ratio of 20:100. The increasing dye concentration increases reabsorption within the sample (see Fig. 4), which reduces the PL intensity at shorter wavelengths. However, Theo-Red has limited solubility in SBS. Therefore the scattering films at high dye content scatter short-wavelength light out of the dye-SBS composite more efficiently than red light, which results in a blue shift of the emission. We also observe a blue shift due to the increase of film polarity for Theo-Red as shown in Fig. S5.3.

9. Fabrication details of solution-processed waveguide and edge-lit device.

In this section, we demonstrate the fabrication of waveguides of different mechanical properties via solution processing. To start with, dyes and a polymer are dissolved into an organic solvent to form a fluorescent solution. The fluorescent solution consisting of the dyes and SBS can be processed into waveguides via blade-coating and procedures are:

1. Dissolve Theo-Green (100 mg), SBS (1 g) into 10 ml toluene.
2. Transfer the obtained solution into a 12 ml syringe and install the syringe onto FOM sheet coater.
3. Preheat glass substrates to 60 °C.
4. Setting solution feeding rate to 10 ml/min and slot die head speed to 70 cm/min.
5. Execute the sheet coating program.

Subsequently, we integrate the glass waveguide with LED strips to form the edge-lit structure shown in Fig. S8.

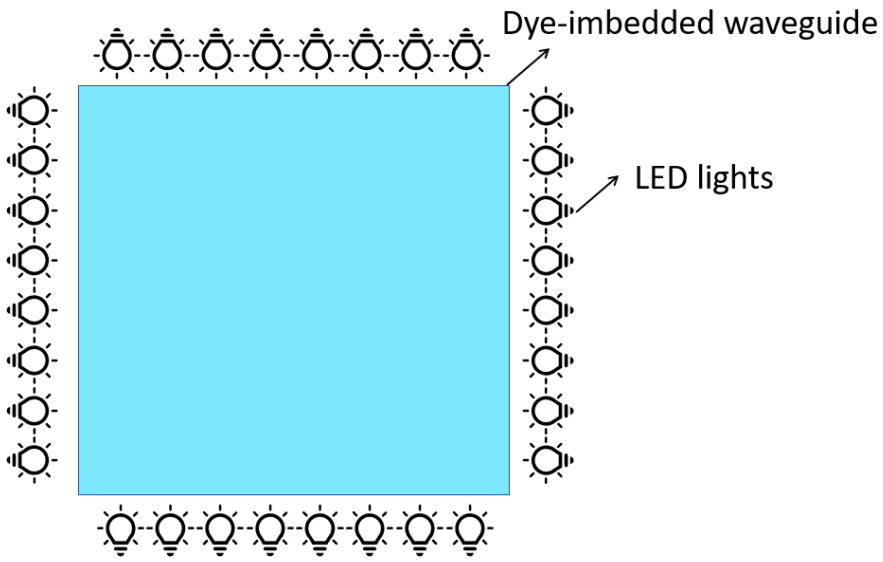

Fig. S9.1. The device structure of an edge-lit transparent non-glare LED enable by a dye-imbedded waveguide.

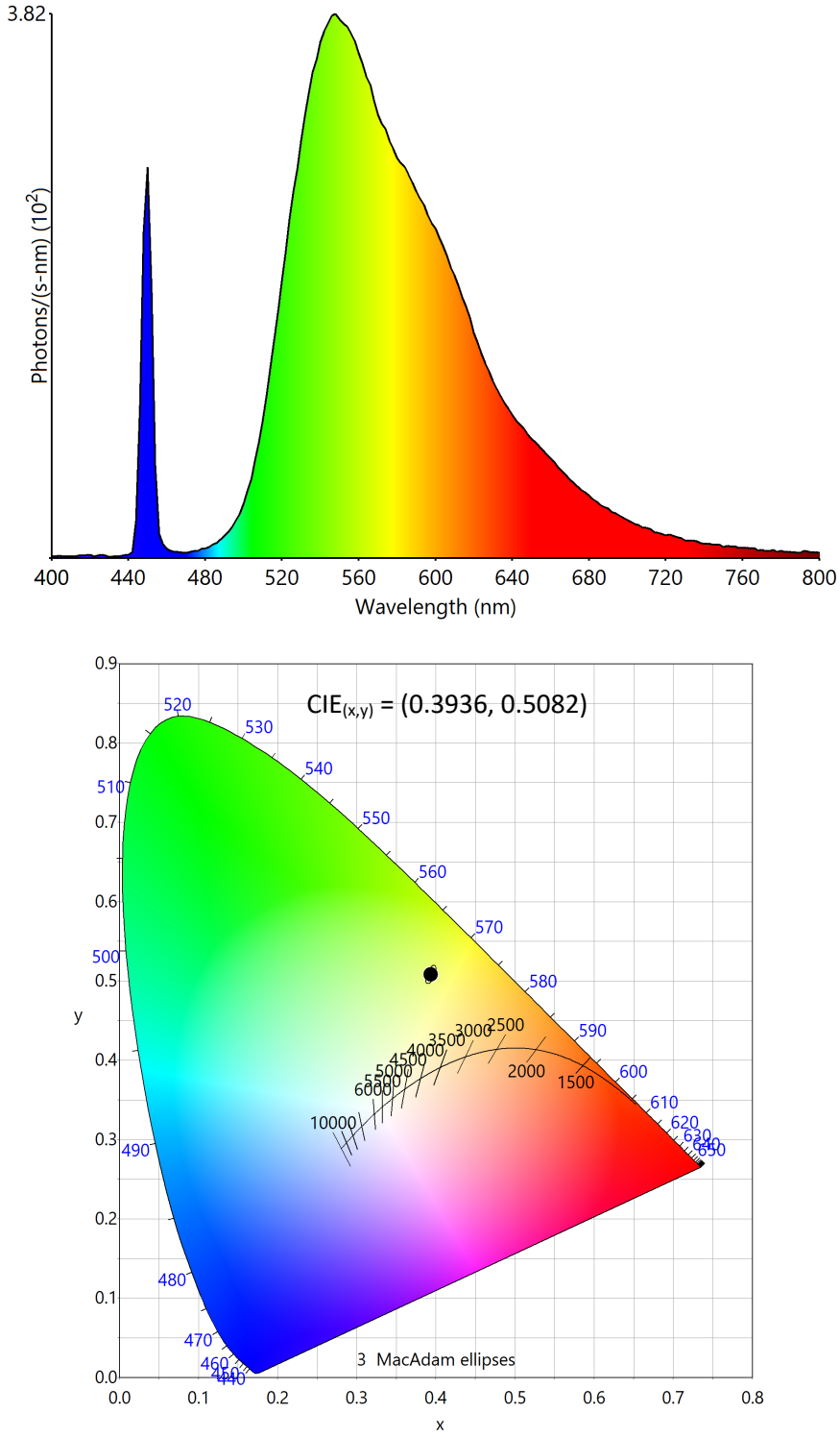

Fig. S9.2. The emission spectra (top) and the CIE coordinate (bottom) of the device.

10. Thermal stability of organic dyes.

Fig. S10 summarizes the thermogravimetric analysis results of the six organic dyes, and their decomposition temperature (threshold set at 95% of the initial weight) are respectively 464 °C for PT4, 453 °C for R305, 321°C for DCJTB, 402 °C for Theo-Green, 408 °C for Theo-Red and 388 °C for BT-TPA. The decomposition temperatures of the theobromine dyes are substantially higher than room temperature, around which the edge-lit device operate in, and therefore the thermal stability of these theobromine dyes is not concerning in this application.

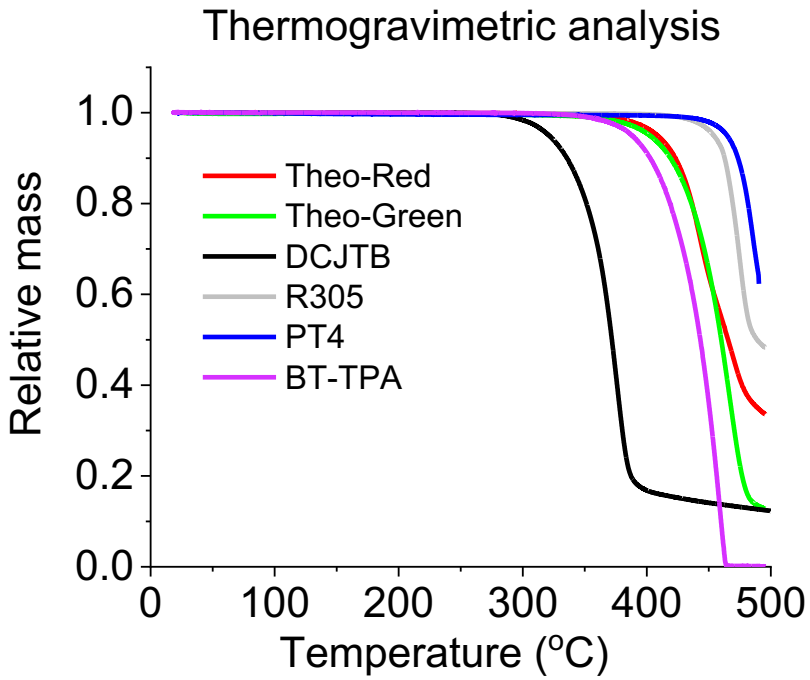

Fig. S10. The thermogravimetric analysis results of the six organic dyes.

11. PLQY comparison of phosphors from different categories.

Table S2. PLQY comparison of current state-of-art phosphors from different categories.

Phosphor(@Matrix)	Catagory	Color	Emission peak [nm]	PLQY/ EQE [%]	Reference
Theo-Green@SBS	**Bio-derived, organic dye**	**Green**	**555**	**94** [a,d]	**This work**
Theo-Red@SBS	**Bio-derived, organic dye**	**Red**	**603**	**87** [a,d]	**This work**
PT4@SBS	Bio-derived, organic dye	Green	516	90 [a,d]	Measured
BT-TPA@SBS	Organic dye	Orange	593	92 [a,d]	Measured
R305@SBS	Organic dye	Red	661	59 [a,d]	Measured
DCJTB@SBS	Organic dye	Red	627	37 [a,d]	Measured
DBQ@3DMAC	Organic dye	Green	551	84 [c,d]	5
TAT−FDBPZ@CBP	Organic dye	Orange	576	62 [b,d]	6
4CzTPNBu@ptBCzPO2TPTZ	Organic dye	Orange	576	90 [b,d]	7
BPPZ-PXZ@CBP	Organic dye	Red	607	100 [b,d]	8
mDPBPZ-PXZ@CBP	Organic dye	Red	638	95 [b,d]	8
DBQ@3PXZ	Organic dye	Red	618	76 [c,d]	5
HAP-3TPA@26mCPy	Organic dye	Red	610	91 [b,d]	9
eGFP-AA@TMPE:PMMA	Bio-derived, fluorescent protein	Green	509	80 [a,d]	10
FP@SF	Bio-derived, fluorescent protein	Green	526	65 [a,d]	11
mCherry@PEO	Bio-derived, fluorescent protein	Red	641	18 [c,d]	12
mScarlet@PDMS	Bio-derived, fluorescent protein	Red	600	70 [c,d]	13
$RbNa(Li_3SiO_4)_2:Eu^{2+}$	Micron-size inorganic phosphor	Green	523	44 [c,e]	14
$La_4GeO_8:Bi^{3+}$	Micron-size inorganic phosphor	Red	600	69 [c,e]	15
$Cs_2SiF_6:Mn^{4+}$	Micron-size inorganic phosphor	Red	632	71 [c,e]	16
$Sr[LiAl_3N_4]:Eu^{2+}$	Micron-size inorganic phosphor	Red	649	74 [c,e]	17
$CsPbBr_3@ZrO_2$	Quantum dots	Green	514	90 [c,d]	18
$CsPbBr_3@SiO_2/Al_2O_3$	Quantum dots	Green	519	90 [c,d]	19
$CsPbBr_3$@ZP3/EVA	Quantum dots	Green	519	93 [a,d]	3
InP/ZnSe/ZnS	Quantum Dots	Green	528	95 [c,d]	21
$CuInSe_xS_{2-x}$/ZnS	Quantum Dots	Green	590	95 [c,d]	22
$Ag_{1.3}In_{4.0}Zn_{1.0}S_{4.9}$	Quantum Dots	Red	623	60 [c,d]	23
$CsPbI_3$@ZP4/EVA	Quantum dots	Red	695	85 [a,d]	3
$CuInSe_xS_{2-x}$/ZnS	Quantum Dots	Red	650	95 [c,d]	22

a) Measured in ambient atmosphere; b) Measured in inert atmosphere; c) Measurement condition unspecified; d) PLQY values; e) EQE values; f) Photothermal threshold quantum yield.

Reference

1. Y. Huang, Y. Liu, P. J. W. Sommerville, W. Kaminsky, D. S. Ginger and C. K. Luscombe, *Green Chem.*, 2019, **21**, 6600.
2. P. Wei, L. Duan, D. Zhang, J. Qiao, L. Wang, R. Wang, G. Dong and Y. Qiu, *J. Mater. Chem.*, 2008, **18**, 806.
3. T. A. Cohen, Y. Huang, N. A. Bricker, C. S. Juhl, T. J. Milstein, J. D. Mackenzie, C. K. Luscombe and D. R. Gamelin, *Chem. Mater.*, 2021, DOI: https://doi.org/10.1021/acs.chemmater.1c00902.
4. W. Fudickar and T. Linker, *J. Am. Chem. Soc.*, 2012, **134**, 15071.
5. L. Yu, Z. Wu, G. Xie, W. Zeng, D. Ma and C. Yang, *Chem. Sci.*, 2018, **9**, 1385.
6. Y. Liu, Y. Chen, H. Li, S. Wang, X. Wu, H. Tong and L. Wang, *ACS Appl. Mater. & Interfaces*, 2020, **12**, 30652.
7. D. Ding, Z. Wang, C. Li, J. Zhang, C. Duan, Y. Wei and H. Xu, *Adv. Mater.*, 2020, **32**, 1906950.
8. J.-X. Chen, W.-W. Tao, W.-C. Chen, Y.-F. Xiao, K. Wang, C. Cao, J. Yu, S. Li, F.-X. Geng, C. Adachi, C.-S. Lee and X.-H. Zhang, *Angew. Chem. Int. Ed.*, 2019, **58**, 14660-14665.
9. J. Li, T. Nakagawa, J. MacDonald, Q. Zhang, H. Nomura, H. Miyazaki and C. Adachi, *Adv. Mater.*, 2013, **25**, 3319.
10. A. Espasa, M. Lang, C. F. Aguiño, D. Sanchez-deAlcazar, J. P. Fernández-Blázquez, U. Sonnewald, A. L. Cortajarena, P. B. Coto and R. D. Costa, *Nat. Comm.*, 2020, **11**, 879.
11. V. Fernández-Luna, J. P. Fernández-Blázquez, M. A. Monclús, F. J. Rojo, R. Daza, D. Sanchez-deAlcazar, A. L. Cortajarena and R. D. Costa, *Mater, Hori.*, 2020, **7**, 1790.
12. L. Niklaus, S. Tansaz, H. Dakhil, K. T. Weber, M. Pröschel, M. Lang, M. Kostrzewa, P. B. Coto, R. Detsch, U. Sonnewald, A. Wierschem, A. R. Boccaccini and R. D. Costa, *Adv. Funct. Mater.*, 2017, **27**, 1601792.
13. S. Sadeghi, R. Melikov, D. Conkar, E. N. Firat-Karalar and S. Nizamoglu, *Adv. Mater. Technol.*, 2020, **5**, 2070035.
14. H. Liao, M. Zhao, Y. Zhou, M. S. Molokeev, Q. Liu, Q. Zhang and Z. Xia, *Adv. Funct. Mater.*, 2019, **29**, 1901988.
15. Y. Wei, G. Xing, K. Liu, G. Li, P. Dang, S. Liang, M. Liu, Z. Cheng, D. Jin and J. Lin, *Light Sci. Appl.*, 2019, **8**, 15.
16. E. Song, Y. Zhou, X.-B. Yang, Z. Liao, W. Zhao, T. Deng, L. Wang, Y. Ma, S. Ye and Q. Zhang, *ACS Photonics*, 2017, **4**, 2556.
17. P. Pust, V. Weiler, C. Hecht, A. Tücks, A. S. Wochnik, A.-K. Henß, D. Wiechert, C. Scheu, P. J. Schmidt and W. Schnick, *Nat. Mater.*, 2014, **13**, 891.
18. H. Liu, Y. Tan, M. Cao, H. Hu, L. Wu, X. Yu, L. Wang, B. Sun and Q. Zhang, *ACS Nano*, 2019, **13**, 5366.
19. Z. Li, L. Kong, S. Huang and L. Li, *Angew. Che. In. Ed.*, 2017, **56**, 8134.
20. Y. Kim, S. Ham, H. Jang, J. H. Min, H. Chung, J. Lee, D. Kim and E. Jang, *ACS Appl. Nano Mater.*, 2019, **2**, 1496.
21. N. S. Makarov, K. Ramasamy, A. Jackson, A. Velarde, C. Castaneda, N. Archuleta, D. Hebert, M. R. Bergren and H. McDaniel, *ACS Nano*, 2019, **13**, 9112.
22. H. Guan, S. Zhao, H. Wang, D. Yan, M. Wang and Z. Zang, *Nano Energy*, 2020, **67**, 104279.